Tunnel magnetoresistance for coherent spin-flip processes on an interacting quantum dot

2009 J. Phys.: Condens. Matter 21 046005

(http://iopscience.iop.org/0953-8984/21/4/046005)

IOP Publishing Journal of Physics: Condensed Matter

J. Phys.: Condens. Matter **21** (2009) 046005 (12pp) doi:10.1088/0953-8984/21/4/046005

Tunnel magnetoresistance for coherent spin-flip processes on an interacting quantum dot

W Rudziński

Department of Physics, Adam Mickiewicz University, ulica Umultowska 85, 61-614 Poznań, Poland

E-mail: wojrudz@amu.edu.pl

Received 10 October 2008, in final form 28 November 2008
Published 8 January 2009
Online at stacks.iop.org/JPhysCM/21/046005

Abstract

Spin-polarized electronic tunneling through a quantum dot coupled to ferromagnetic electrodes is investigated within a nonequilibrium Green function approach. An interplay between coherent intradot spin-flip transitions, tunneling processes and Coulomb correlations on the dot is studied for current–voltage characteristics of the tunneling junction in parallel and antiparallel magnetic configurations of the leads. It is found that due to the spin-flip processes electric current in the antiparallel configuration tends to the current characteristics in the parallel configuration, thus giving rise to suppression of the tunnel magnetoresistance (TMR) between the threshold bias voltages at which the dot energy level becomes active in tunneling. Also, the effect of a negative differential conductance in symmetrical junctions, splitting of the conductance peaks, significant modulation of TMR peaks around the threshold bias voltages as well as suppression of the diode-like behavior in asymmetrical junctions is discussed in the context of coherent intradot spin-flip transitions. It is also shown that TMR may be inverted at selected gate voltages, which qualitatively reproduces the TMR behavior predicted recently for temperatures in the Kondo regime, and observed experimentally beyond the Kondo regime for a semiconductor InAs quantum dot coupled to nickel electrodes.

(Some figures in this article are in colour only in the electronic version)

1. Introduction

Coherent manipulation of the charge states in nano-scale devices is crucial for future spintronics and quantum information data processing (see e.g. [1–3]). In particular, progress in nanofabrication technology has stimulated both theoretical and experimental studies on understanding intrinsic spin relaxation mechanisms as well as effects due to coherent spin-flip processes in mesoscopic systems [1, 4–28]. A device that is most widely used in these investigations consists of a quantum dot (QD) coupled to external electrodes through tunneling barriers.

Experimentally, intradot spin-flip phenomena have been investigated in semiconductor GaAs, InAs and InGaAs QDs to measure spin relaxation and spin decoherence times [1, 9, 13, 15–18, 20, 21, 24, 25, 27]. In particular, it is indicated that spin flips and spin decoherence are dominated by spin–orbit interactions and hyperfine coupling to lattice nuclear spins. Also, a number of successful attempts at spin manipulation in the considered semiconductor QDs have been reported [9, 18, 27].

Theoretical investigations on spin-flip transitions in GaAs-based QDs have revealed that spin–orbit coupling may cause the spin rotation of an electron while in a QD [5]. Regarding the dynamics of electron spins coupled to nuclei, a detailed theory describing the properties of coupled electrons in double QDs has been proposed to guide experiments on coherent spin manipulation of electron spins [26]. In turn, for hybrid ferromagnetic QD–superconductor tunneling junctions a novel double-peak structure in the Andreev reflection conductance spectrum has been predicted to occur for strong enough spin-flip scattering [12].

Another important element of theories so far is the investigation of the influence of intradot spin-flip transitions

on current–voltage (I–V) characteristics in magnetic tunnel junctions. When both external leads are ferromagnetic, then the basic spin-dependent property in such a junction is the tunnel magnetoresistance (TMR). This feature appears as a change in the junction resistance when magnetic moments of external electrodes are switched between the parallel (P) alignment and the antiparallel (AP) one. The TMR effect is known to occur in planar junctions [29–31], granular systems [20, 32, 33] and carbon nanotubes [2], and has been also predicted to appear in mesoscopic double-barrier junctions based on QDs [34–50]. Recently, the first demonstration of the gate-tunable memory effect has been reported for a spin-valve device consisting of a self-assembled InAs quantum dot with ferromagnetic Co and Ni leads [51, 52]. In particular, it has been revealed that in the vicinity of the Coulomb blockade conductance peak, the TMR may be significantly modulated and even its sign can be switched by changing the gate voltage.

The effect of spin-flip transitions is known to reduce the TMR for a quantum dot in the sequential tunneling regime [6]. At low temperatures in the Kondo regime it is also found that the zero bias TMR becomes negative with increasing spin-flip transition amplitude [7, 8]. The latter property is accompanied by suppression of the Kondo effect with simultaneous splitting of the Kondo resonance into the well-defined three and two peaks in the parallel and antiparallel configuration, respectively. Inverse tunnel magnetoresistance has been also observed for fast intradot intrinsic spin relaxation occurring in the co-tunneling regime [22]. Within the same investigation an interesting effect of spin relaxation-induced enhancement of the diode-like behavior has been predicted for quantum dots asymmetrically coupled to the ferromagnetic leads.

In this paper an effect of coherent intradot spin-flip processes on electric current and TMR is considered for spin-polarized electronic transport through quantum dots weakly coupled to external ferromagnetic electrodes, i.e. the focus is on spin-polarized tunneling at temperatures above the Kondo limit. The situation when the spin-flip scattering strength overwhelms that of the tunneling coupling is analyzed, which may originate either from the transverse component of an applied magnetic field or from tunable spin–orbit coupling of the Rashba–Dresselhaus type in the dot (see e.g. [54–56]). What is important is that the considered spin-flip transitions lift the degeneracy of the discrete dot level thus giving rise to new features of the current–voltage characteristics for the tunneling junction.

The aim of the present paper is to discuss different aspects of the spin-valve phenomenon in systems based on QDs, in the context of an interplay between intradot spin-flip transitions, tunneling processes and Coulomb correlations on the dot. The most spectacular effects due to the spin-flip transitions are expected to occur in spintronic devices working as a perfect spin valve or as a mesoscopic diode. In the former case the question of mechanism of reduction of the maximum TMR ratio for a dot coupled to half-metallic electrodes arises when the spin-flip processes take place. As for the nano-scale current rectification effect, an important condition for the diode-like behavior is the degeneracy of the ground state of the quantum dot. This spin degeneracy is lifted when an electron may tunnel into the superposition of the up- and down-spin states on the dot. Thus, the question of modification of the diode characteristics arises in the case when the coherent spin-flip transitions are allowed to occur on the dot.

In order to calculate the electric current and TMR we employ the nonequilibrium Green function technique, using the equation of motion method in the Hartree–Fock approximation. In contrast to the previous theoretical attempts at studying the spin-flip effects in QDs, based on the master equation or on the second-order perturbation method [6, 22], the approach used here allows for the spin-flip transitions to be analyzed in both sequential and higher-order tunneling regimes. The many-body approach used here also allows for numerical detection of the intradot Larmor precession of an electron spin around an axis perpendicular to the easy axis of the external leads [57]. The magnitude of such a spin precession in the presence of coherent rotation of electron spin on the dot may be readily evaluated within the self-consistent Green function calculation.

The paper is organized as follows. In section 2 we describe a model of the system. The theoretical method is described in section 3, where the equation of motion method is used to derive nonequilibrium Green functions of the dot. Next, the Green functions are used to calculate transport characteristics for the system. Relevant numerical results for the tunneling current, conductance and magnetoresistance as well as averages of the spin components on the dot are presented and discussed in section 4. Finally, a summary and general conclusions are given in section 5.

2. Model

We consider a single-level quantum dot coupled to two ferromagnetic leads via tunneling barriers. The whole system can be described by a Hamiltonian of the general form

$$H = H_{\mathrm{l}} + H_{\mathrm{r}} + H_{\mathrm{d}} + H_{\mathrm{t}}. \tag{1}$$

The term H_ν describes the left ($\nu = \mathrm{l}$) and right ($\nu = \mathrm{r}$) electrodes in the non-interacting quasi-particle approximation

$$H_\nu = \sum_{k,\sigma} \varepsilon^\nu_{k\sigma} a^\dagger_{\nu k\sigma} a_{\nu k\sigma}, \tag{2}$$

where $\varepsilon^\nu_{k\sigma}$ is the single-electron energy in the νth electrode for the wavevector k and spin σ ($\sigma = \uparrow, \downarrow$), whereas $a^\dagger_{\nu k\sigma}$ and $a_{\nu k\sigma}$ are the corresponding creation and annihilation operators. Note moreover that both the ferromagnetic leads are assumed to possess the same easy axis along the z-direction. The term H_{d} in equation (1) describes the quantum dot

$$H_{\mathrm{d}} = \varepsilon_{\mathrm{d}} \sum_\sigma c^\dagger_\sigma c_\sigma + U c^\dagger_\uparrow c_\uparrow c^\dagger_\downarrow c_\downarrow + R(c^\dagger_\uparrow c_\downarrow + c^\dagger_\downarrow c_\uparrow), \tag{3}$$

where ε_{d} denotes the energy of the discrete level, which is doubly degenerate in the spin index σ, U is the electron correlation parameter and $c^\dagger_\sigma$ and c_σ are the creation and annihilation operators, respectively, for electrons with spin orientation $\sigma = \uparrow$ ($\downarrow$). The parameter R in equation (3)

describes the phenomenological spin-flip transition amplitude. The spin-flip term is assumed to be coherent, in the sense that the spin-flip strength R involves reversible transitions between up- and down-spin states on the dot. Such an effect may originate from a spin–orbit coupling in the dot or from the transverse component of a local magnetic field applied, for example, within the electron spin resonance technique [3, 58].

Finally, the tunneling part of the model Hamiltonian (1) takes the form

$$H_{\rm t} = \sum_{\nu,k,\sigma} T^{\nu}_{k\sigma} a^{\dagger}_{\nu k\sigma} c_{\sigma} + {\rm h.c.}, \tag{4}$$

where $T^{\nu}_{k\sigma}$ ($\nu = {\rm l}, {\rm r}$) is the tunneling amplitude and h.c. stands for the Hermitian conjugate terms.

As stated above, the spin quantization axes in the external electrodes are fixed parallel to the z-direction of the Cartesian coordinate system by the internal magnetization of the ferromagnets. It indicates that the incident electrons with up-spin and down-spin from the source lead should tunnel coherently onto the discrete level split by the intradot spin flips. This tunneling of electrons into a superposition of spin-up and spin-down states may be introduced by using spin rotation transformation [7]:

$$d_{\uparrow(\downarrow)} = \frac{1}{\sqrt{2}}(c_{\uparrow} \pm c_{\downarrow}). \tag{5}$$

Thus, the dot Hamiltonian (3) is reshaped into the following form

$$H_{\rm d} = \sum_{\sigma} \varepsilon_{{\rm d}\sigma} d^{\dagger}_{\sigma} d_{\sigma} + U d^{\dagger}_{\uparrow} d_{\uparrow} d^{\dagger}_{\downarrow} d_{\downarrow}, \tag{6}$$

with

$$\varepsilon_{{\rm d}\uparrow(\downarrow)} = \varepsilon_{\rm d} \mp R, \tag{7}$$

whereas the tunneling Hamiltonian (4) becomes

$$H_{\rm t} = \frac{1}{\sqrt{2}} \sum_{\nu,k,\sigma} \left(T^{\nu}_{k\uparrow} a^{\dagger}_{\nu k\uparrow} + (-1)^{\delta_{\uparrow\sigma}} T^{\nu}_{k\downarrow} a^{\dagger}_{\nu k\downarrow} \right) {\rm d}_{\sigma} + {\rm h.c.} \tag{8}$$

3. Green function formalism

To calculate electric current in the nonequilibrium situation we make use of the nonequilibrium Green function defined on the Keldysh contour [60]. Accordingly, we introduce the causal (time-ordered) Green function of the dot, $G_{\sigma\sigma'}(t) \equiv -{\rm i}\langle T[d_{\sigma}(t), d^{\dagger}_{\sigma'}(0)]\rangle$, as well as the lesser correlation Green function defined as $G^{<}_{\sigma\sigma'}(t) \equiv {\rm i}\langle d^{\dagger}_{\sigma'}(0) d_{\sigma}(t)\rangle$. The explicit expression for these Green functions can be obtained by using the equation of motion method. The equation of motion for the Fourier transforms of the causal correlators defined as $G_{\sigma\sigma'}(\epsilon) \equiv \langle\langle d_{\sigma} \,|\, d^{\dagger}_{\sigma'}\rangle\rangle_{\epsilon}$ reads

$$\begin{aligned}(\epsilon - \epsilon_{\rm d})\langle\langle d_{\sigma} \,|\, d^{\dagger}_{\sigma'}\rangle\rangle_{\epsilon} &= \delta_{\sigma\sigma'} \\ &+ \sum_{k,\nu} [T^{*\nu}_{k\sigma} \langle\langle a_{\nu k\sigma} \,|\, d^{\dagger}_{\sigma'}\rangle\rangle_{\epsilon} + (-1)^{\delta_{\uparrow\sigma}} T^{*\nu}_{k-\sigma} \langle\langle a_{\nu k-\sigma} \,|\, d^{\dagger}_{\sigma'}\rangle\rangle_{\epsilon}] \\ &+ U \langle\langle d_{\sigma} d^{\dagger}_{-\sigma} d_{-\sigma} \,|\, d^{\dagger}_{\sigma'}\rangle\rangle_{\epsilon}. \end{aligned} \tag{9}$$

Applying the equation of motion to the three new Green functions on the r.h.s. of equation (9), one finds

$$(\epsilon - \varepsilon^{\nu}_{k\pm\sigma})\langle\langle a_{\nu k\pm\sigma} \,|\, d^{\dagger}_{\sigma'}\rangle\rangle_{\epsilon} = \frac{1}{\sqrt{2}} T^{\nu}_{k\pm\sigma} \left[\langle\langle d_{\pm\sigma} \,|\, d^{\dagger}_{\sigma'}\rangle\rangle_{\epsilon} + (-1)^{\delta_{\downarrow\sigma}} \langle\langle d_{\mp\sigma} \,|\, d^{\dagger}_{\sigma'}\rangle\rangle_{\epsilon} \right], \tag{10}$$

$$\begin{aligned}(\epsilon - \epsilon_{{\rm d}\sigma} - U)\langle\langle d_{\sigma} d^{\dagger}_{-\sigma} d_{-\sigma} \,|\, d^{\dagger}_{\sigma'}\rangle\rangle_{\epsilon} &= \langle\{d_{\sigma} d^{\dagger}_{-\sigma} d_{-\sigma}, d^{\dagger}_{\sigma'}\}\rangle \\ &+ \frac{\langle d^{\dagger}_{-\sigma} d_{-\sigma}\rangle}{\sqrt{2}} \sum_{k\nu} [T^{*\nu}_{k\sigma} \langle\langle a_{\nu k\sigma} \,|\, d^{\dagger}_{\sigma'}\rangle\rangle_{\epsilon} \\ &- T^{*\nu}_{k-\sigma} \langle\langle a_{\nu k-\sigma} \,|\, d^{\dagger}_{\sigma'}\rangle\rangle_{\epsilon}] \\ &- \frac{\langle d^{\dagger}_{-\sigma} d_{\sigma}\rangle}{\sqrt{2}} \sum_{k\nu} [T^{*\nu}_{k\sigma} \langle\langle a_{\nu k\sigma} \,|\, d^{\dagger}_{\sigma'}\rangle\rangle_{\epsilon} \\ &+ T^{*\nu}_{k-\sigma} \langle\langle a_{\nu k-\sigma} \,|\, d^{\dagger}_{\sigma'}\rangle\rangle_{\epsilon}]. \end{aligned} \tag{11}$$

In obtaining the equation of motion (11) for the higher-order Green function we have neglected correlations involving lead electrons and the Hartree–Fock decoupling scheme was applied, $\langle\langle a_{\nu k\sigma}\, d^{\dagger}_{-\sigma} d_{\pm\sigma} \,|\, c^{\dagger}_{\sigma'}\rangle\rangle_{\epsilon} \rightarrow \langle d^{\dagger}_{-\sigma} d_{\pm\sigma}\rangle \langle\langle a_{\nu k\sigma} \,|\, c^{\dagger}_{\sigma'}\rangle\rangle_{\epsilon}$, where $\langle\cdots\rangle$ means the quantum statistical average value of the appropriate operator. This approximation closes the set of equations (9)–(11) allowing us to find a solution for the causal Green functions $G_{\sigma\sigma'}(\epsilon)$

$$\mathbf{G}(\epsilon) = \begin{bmatrix} G_{\uparrow\uparrow}(\epsilon) & G_{\uparrow\downarrow}(\epsilon) \\ G_{\downarrow\uparrow}(\epsilon) & G_{\downarrow\downarrow}(\epsilon) \end{bmatrix}, \tag{12}$$

from the Dyson matrix equation

$$\mathbf{G}(\epsilon) = \left[\mathbf{1} - \mathbf{g}^{(0)}(\epsilon)\mathbf{\Sigma}(\epsilon)\right]^{-1} \mathbf{g}^{(0)}(\epsilon), \tag{13}$$

where $\mathbf{g}^{(0)}(\epsilon)$ is the Green function of the dot in the absence of Coulomb correlation and coupling to the leads, $g^{(0)}_{\sigma\sigma'}(\epsilon) = \delta_{\sigma\sigma'}(\epsilon - \varepsilon_{{\rm d}\sigma})^{-1}$, and where $\mathbf{\Sigma}(\epsilon)$ is the self-energy given by

$$\mathbf{\Sigma}(\epsilon) = \begin{bmatrix} \Sigma_1(\epsilon) & \Sigma_2(\epsilon) \\ \Sigma_2(\epsilon) & \Sigma_1(\epsilon) \end{bmatrix}, \tag{14}$$

with

$$\Sigma_{1,2}(\epsilon) = \frac{1}{2} \sum_{k,\nu} \left[\frac{|T^{\nu}_{k\uparrow}|^2}{\epsilon - \varepsilon^{\nu}_{k\uparrow}} \pm \frac{|T^{\nu}_{k\downarrow}|^2}{\epsilon - \varepsilon^{\nu}_{k\downarrow}} \right]. \tag{15}$$

Finally one finds the explicit expressions for the causal Green functions:

$$G_{\sigma\sigma}(\epsilon) = \frac{A_{\sigma\sigma} g_{\sigma\sigma}(\epsilon) + B_{\sigma\sigma} g_{-\sigma\sigma}(\epsilon)}{A_{\sigma\sigma} A_{-\sigma-\sigma} - B_{\sigma\sigma} B_{-\sigma-\sigma}}, \tag{16}$$

$$G_{-\sigma\sigma}(\epsilon) = \frac{A_{\sigma\sigma} g_{-\sigma\sigma}(\epsilon) + B_{-\sigma-\sigma} g_{\sigma\sigma}(\epsilon)}{A_{\sigma\sigma} A_{-\sigma-\sigma} - B_{\sigma\sigma} B_{-\sigma-\sigma}}, \tag{17}$$

where

$$A_{\sigma\sigma} = 1 - g_{-\sigma-\sigma}(\epsilon)\Sigma_1(\epsilon) - g_{-\sigma\sigma}(\epsilon)\Sigma_2(\epsilon), \tag{18}$$

$$B_{\sigma\sigma} = g_{\sigma\sigma}(\epsilon)\Sigma_2(\epsilon) + g_{\sigma-\sigma}(\epsilon)\Sigma_1(\epsilon) \tag{19}$$

with

$$g_{\sigma\sigma}(\epsilon) = \frac{\epsilon - \varepsilon_{{\rm d}\sigma} - U(1 - \langle d^{\dagger}_{-\sigma} d_{-\sigma}\rangle)}{(\epsilon - \varepsilon_{{\rm d}\sigma})(\epsilon - \varepsilon_{{\rm d}\sigma} - U)}, \tag{20}$$

$$g_{\sigma-\sigma}(\epsilon) = -\frac{U\langle d^{\dagger}_{-\sigma}d_{\sigma}\rangle}{(\epsilon-\varepsilon_{\mathrm{d}\sigma})(\epsilon-\varepsilon_{\mathrm{d}\sigma}-U)}. \tag{21}$$

The retarded self-energies (15) are given by the formulae

$$\Sigma_{1,2}(\epsilon) = \frac{1}{2}\sum_{\nu}\left[\Gamma^{\nu}_{\uparrow}(\epsilon)\pm\Gamma^{\nu}_{\downarrow}(\epsilon)\right]\left[\frac{1}{\pi}\ln\left(\frac{D+eV_{\nu}-\epsilon}{D-eV_{\nu}+\epsilon}\right)+i\right], \tag{22}$$

where

$$\Gamma^{\nu}_{\uparrow(\downarrow)}(\epsilon) = 2\pi\sum_{k}|T^{\nu}_{k\uparrow(\downarrow)}|^2\delta(\epsilon-\epsilon^{\nu}_{k\uparrow(\downarrow)}) \tag{23}$$

for $\nu = \mathrm{l}, \mathrm{r}$. It has been assumed that the lower and upper edges of the electron band at zero bias are at $-D$ and D, respectively. In the following we assume

$$\Gamma^{\mathrm{l}}_{\uparrow(\downarrow)}(\epsilon) = \Gamma^{\mathrm{l}}_{\uparrow(\downarrow)} = \Gamma_0(1\pm p_{\mathrm{l}}) \tag{24}$$

and

$$\Gamma^{\mathrm{r}}_{\uparrow(\downarrow)}(\epsilon) = \Gamma^{\mathrm{r}}_{\uparrow(\downarrow)} = \alpha\Gamma_0(1\pm p_{\mathrm{r}}) \tag{25}$$

when ϵ is within the electron band and zero otherwise. The parameters p_{l} and p_{r} describe the spin asymmetry of the coupling to the left and right electrodes, and Γ_0 determines the tunneling rate in the case when $p_{\nu} = 0$. Apart from this, the parameter α in the above formula takes into account asymmetry between coupling of the dot to the left and right electrodes.

Since the self-energies given explicitly by equation (22) are independent of U, then one can compute exactly the density matrix in the spin space, using the Keldysh equation for the correlation function $\mathbf{G}^{<}(\epsilon)$

$$\mathbf{G}^{<}(\epsilon) = \mathbf{G}^{\mathrm{R}}(\epsilon)\mathbf{\Sigma}^{<}(\epsilon)\mathbf{G}^{\mathrm{A}}(\epsilon), \tag{26}$$

where $\mathbf{G}^{\mathrm{R(A)}}(\epsilon)$ are the retarded (advanced) Green functions, $G^{\mathrm{R(A)}}_{\sigma\sigma'}(\epsilon) = G_{\sigma\sigma'}(\epsilon\pm\mathrm{i}\eta)$, and where

$$\mathbf{\Sigma}^{<}(\epsilon) = -\sum_{\nu}[\mathbf{\Sigma}^{R}_{\nu}(\epsilon)-\mathbf{\Sigma}^{A}_{\nu}(\epsilon)]f_{\nu}(\epsilon). \tag{27}$$

The quantities $\mathbf{\Sigma}^{\mathrm{R(A)}}_{\nu}(\epsilon)$ in equation (27) are the retarded (advanced) self-energies and $f_{\nu}(\epsilon)$ denotes the Fermi–Dirac distribution function for the νth electrode, $f_{\nu}(\epsilon) = 1/\{1+\exp[(\epsilon-\mu_{\nu})/k_{\mathrm{B}}T]\}$, with the electrochemical potentials $\mu_{\mathrm{l}} = eV_{\mathrm{l}} = eV/2$ and $\mu_{\mathrm{r}} = eV_{\mathrm{r}} = -eV/2$.

The average values of the occupation numbers $\langle d^{\dagger}_{\sigma}d_{\sigma}\rangle$ and $\langle d^{\dagger}_{-\sigma}d_{\sigma}\rangle$, which enter the expressions for Green functions, have to be calculated self-consistently by using the lesser Green function as

$$\langle d^{\dagger}_{\sigma}d_{\sigma}\rangle = \mathrm{Im}\int_{-\infty}^{+\infty}\frac{\mathrm{d}\epsilon}{2\pi}G^{<}_{\sigma\sigma}(\epsilon) \tag{28}$$

and

$$\langle d^{\dagger}_{\sigma}d_{-\sigma}\rangle = -\mathrm{i}\int_{-\infty}^{+\infty}\frac{\mathrm{d}\epsilon}{2\pi}G^{<}_{-\sigma\sigma}(\epsilon). \tag{29}$$

After obtaining these statistical averages, one then proceeds to calculate the average values of the spin components accumulated on the dot due to electron tunneling accompanied by the intradot spin-flip processes. These components can be derived from the diagonal and off-diagonal occupation numbers (28) and (29), and in the units of $\hbar$ are given by the formulae

$$\langle S_z\rangle = (n_{\uparrow}-n_{\downarrow})/2, \tag{30}$$

$$\langle S_y\rangle = \mathrm{Im}(n_{\uparrow\downarrow}), \tag{31}$$

$$\langle S_x\rangle = \mathrm{Re}(n_{\uparrow\downarrow}), \tag{32}$$

where for simplicity we have defined $\langle d^{\dagger}_{\sigma}d_{\sigma}\rangle \equiv n_{\sigma}$ and $\langle d^{\dagger}_{\sigma}d_{-\sigma}\rangle \equiv n_{\sigma-\sigma}$.

Spin-polarized electric current flowing from the νth lead to the dot is given by the formula [60]

$$J_{\nu} = \frac{\mathrm{i}e}{\hbar}\int_{-\infty}^{+\infty}\frac{\mathrm{d}\epsilon}{2\pi}\mathrm{Tr}\left\{\mathbf{\Gamma}_{\nu}(\mathbf{G}^{<}(\epsilon)+f_{\nu}(\epsilon)[\mathbf{G}^{\mathrm{R}}(\epsilon)-\mathbf{G}^{\mathrm{A}}(\epsilon)])\right\} \tag{33}$$

with

$$\mathbf{\Gamma}_{\mathrm{l}} = \Gamma_0\begin{pmatrix}1+p_{\mathrm{l}} & 0\\ 0 & 1-p_{\mathrm{l}}\end{pmatrix} \tag{34}$$

and

$$\mathbf{\Gamma}_{\mathrm{r}} = \Gamma_0\alpha\begin{pmatrix}1\pm p_{\mathrm{r}} & 0\\ 0 & 1\mp p_{\mathrm{r}}\end{pmatrix} \tag{35}$$

where the upper and lower signs in (35) correspond to parallel and antiparallel alignment of the lead magnetizations, respectively. Taking into account (16)–(27) together with (33)–(35) one obtains the final expression for the symmetrized electric current in the P(AP) configuration, $J^{\mathrm{P(AP)}} = (1/2)(J^{\mathrm{P(AP)}}_{\mathrm{l}} - J^{\mathrm{P(AP)}}_{\mathrm{r}})$:

$$J^{\mathrm{P(AP)}} = \frac{e\alpha\Gamma_0^2}{4\pi\hbar}\int_{-\infty}^{+\infty}\mathrm{d}\epsilon[f_{\mathrm{l}}(\epsilon)-f_{\mathrm{r}}(\epsilon)]j^{\mathrm{P(AP)}}(\epsilon), \tag{36}$$

with

$$\begin{aligned}j^{\mathrm{P(AP)}}(\epsilon) = {} & (p_{\mathrm{l}}\pm p_{\mathrm{r}})[G^{\mathrm{R}}_{\uparrow\uparrow}(\epsilon)G^{\mathrm{R}*}_{\uparrow\uparrow}(\epsilon)+G^{\mathrm{R}}_{\uparrow\downarrow}(\epsilon)G^{\mathrm{R}*}_{\uparrow\downarrow}(\epsilon)\\ & -G^{\mathrm{R}}_{\downarrow\uparrow}(\epsilon)G^{\mathrm{R}*}_{\downarrow\uparrow}(\epsilon)-G^{\mathrm{R}}_{\downarrow\downarrow}(\epsilon)G^{\mathrm{R}*}_{\downarrow\downarrow}(\epsilon)]\\ & \pm p_{\mathrm{l}}p_{\mathrm{r}}[G^{\mathrm{R}}_{\uparrow\uparrow}(\epsilon)G^{\mathrm{R}*}_{\uparrow\downarrow}(\epsilon)+G^{\mathrm{R}}_{\uparrow\downarrow}(\epsilon)G^{\mathrm{R}*}_{\uparrow\uparrow}(\epsilon)\\ & -G^{\mathrm{R}}_{\downarrow\uparrow}(\epsilon)G^{\mathrm{R}*}_{\downarrow\downarrow}(\epsilon)-G^{\mathrm{R}}_{\downarrow\downarrow}(\epsilon)G^{\mathrm{R}*}_{\downarrow\uparrow}(\epsilon)]\\ & +2[G^{\mathrm{R}}_{\uparrow\uparrow}(\epsilon)G^{\mathrm{R}*}_{\uparrow\uparrow}(\epsilon)+G^{\mathrm{R}}_{\uparrow\downarrow}(\epsilon)G^{\mathrm{R}*}_{\uparrow\downarrow}(\epsilon)+G^{\mathrm{R}}_{\downarrow\uparrow}(\epsilon)G^{\mathrm{R}*}_{\downarrow\uparrow}(\epsilon)\\ & +G^{\mathrm{R}}_{\downarrow\downarrow}(\epsilon)G^{\mathrm{R}*}_{\downarrow\downarrow}(\epsilon)],\end{aligned} \tag{37}$$

as well as the corresponding tunnel magnetoresistance defined as

$$\mathrm{TMR} = \frac{J^{P}-J^{\mathrm{AP}}}{J^{\mathrm{AP}}}. \tag{38}$$

4. Numerical results

4.1. Maps of the electric current, conductance and TMR in the $(eV$–$\varepsilon_{\mathrm{d}})$-plane

Let us first explore features of electric current, differential conductance and TMR shown in figure 1. The presented maps are calculated for a symmetric tunneling junction, i.e. the single-level QD is coupled to identical ferromagnets, $p_{\mathrm{l}} = p_{\mathrm{r}}$, via equivalent barriers, $\alpha = 1$. The transport characteristics under discussion are displayed in the $(eV$–$\varepsilon_{\mathrm{d}})$-plane. When

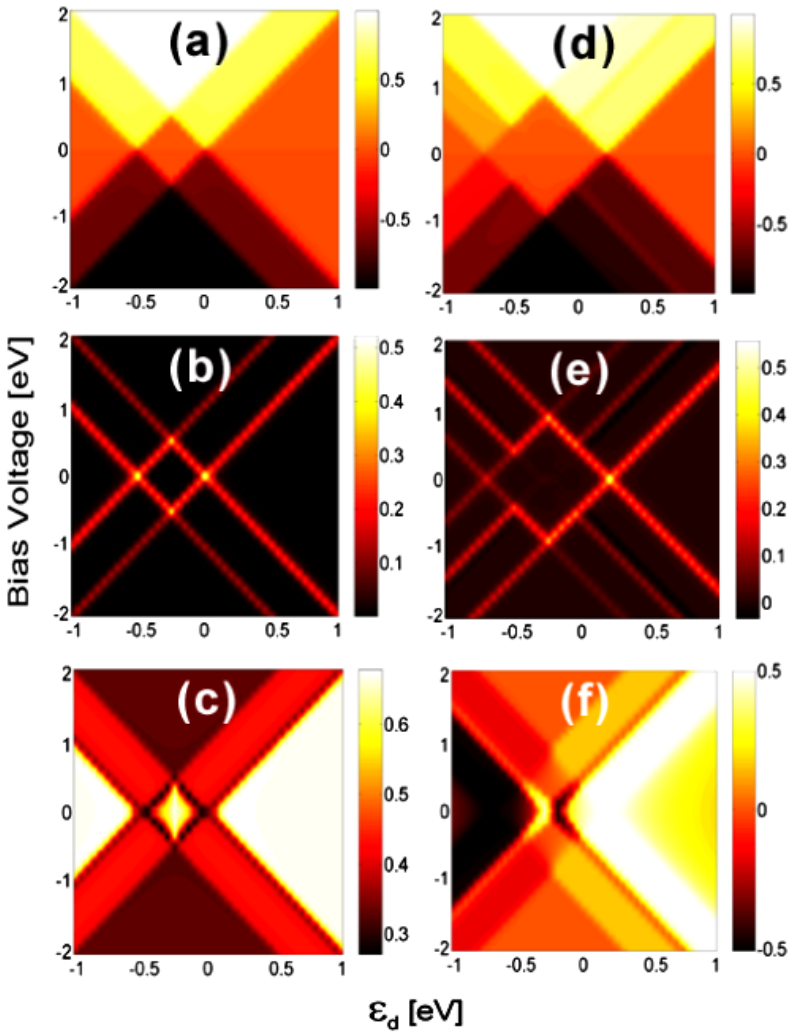

Figure 1. Maps of electric current ((a), (d)), differential conductance ((b), (e)) and TMR ((c), (f)) as a function of the transport bias voltage and the quantum dot energy level ($\varepsilon_{\rm d}$) calculated for a symmetric junction. The electric currents (in units of $e\alpha\Gamma_0/\hbar$) and the corresponding conductances (in units of $2e^2/h$) are displayed for the parallel configuration of magnetic moments in the leads. The transport characteristics of the system without spin-flip transitions, $R = 0$ ((a)–(c)), are compared to the same quantities in the system with non-zero intradot spin-flip strength, $R = 0.2$ eV ((d)–(f)). The other parameters are $p_l = p_r = 0.5$, $\alpha = 1$, $U = 0.5$ eV, $\Gamma_0 = 0.01$ eV and $T = 100$ K.

spin flips on the dot are negligible, $R = 0$, the dot may be empty, single or, due to finite Coulomb correlations on the dot, doubly occupied, thus giving rise to the two steps (visible in figure 1(a)) in the current at bias voltages at which $\varepsilon_{\rm d}$ and $\varepsilon_{\rm d} + U$ cross the Fermi level of the source electrode. The above occurs for all the $\varepsilon_{\rm d}$ dot level positions in equilibrium, except for the specific case of $\varepsilon_{\rm d} = -U/2$. The border lines in the current map also define the Coulomb blockade diamonds, where sequential tunneling processes are exponentially suppressed. The steps in the current at threshold bias voltages determine the positions of the conductance peaks, which form the lines visible on the map in figure 1(b). A similar qualitative picture as in figures 1(a) and (b) is obtained for the current and conductance in the AP configuration. Hence, the TMR ratio may be evaluated from the formula (38). As shown in figure 1(c), the TMR quantity exhibits two essential features. First, TMR is positive in the whole (eV–$\varepsilon_{\rm d}$)-plane; second, TMR is oscillating along both axes, being suppressed or enhanced depending on bias voltage and on the position of the discrete level. In the linear response regime TMR is enhanced in the whole $\varepsilon_{\rm d}$ range except for the resonances at $\varepsilon_{\rm d} = 0$ and $\varepsilon_{\rm d} = -U$, at which the corresponding linear conductance experiences maxima. In the nonequilibrium situation TMR has a broad maximum in the Coulomb blockade regime, in the bias voltage range below the first threshold, arising due to higher-order tunneling processes. In turn, the TMR maximum in the sequential tunneling regime appears when the dot is singly occupied, i.e. when only the level ε_d is in the tunneling window. In this situation, the difference in spin asymmetry for tunneling rates in the AP configuration leads to a difference in occupancy of the dot by majority and minority electrons, $n_\uparrow > n_\downarrow$. By contrast, in the P configuration one has $n_\uparrow = n_\downarrow$. Effectively, this property gives rise to suppression of electric current in the AP configuration relative to the current flowing in the P case so that, in accordance with equation (38), it leads to enhancement of the TMR ratio. When the level $\varepsilon_{\rm d} + U$ also enters the tunneling window, the dot may become doubly occupied,

which means that two electrons with opposite spins may tunnel through the junction. The current enhancement in both P and AP configurations results finally in a significant TMR suppression above the second threshold bias voltage.

When we consider the spin-flip transitions on the dot, then in general one should expect that these processes reduce the differences between the occupation numbers $n_\uparrow$ and $n_\downarrow$. Then, with increasing R the electric current in the AP configuration should tend to the current flowing in the parallel case, thus reducing TMR. Figure 1(f) reveals such a reduction of TMR in the Coulomb blockade as well as in the sequential tunneling regime. Besides, a number of new effects in the transport characteristics in figures 1(d)–(f) are also visible. It is clearly seen in figure 1(d) that additional steps appear in the current, which correspondingly resize the Coulomb blockade diamond areas. One may better understand the origin of this property using the map in figure 1(e), where the system of distinct lines indicates the positions of the differential conductance peaks. Each pair of the conductance maxima is split at the distance $2R$ and these split peaks are positioned symmetrically around the threshold bias voltages. Notice also that when the dot discrete level in equilibrium lies above the Fermi level of the electrodes, $\varepsilon_d > 0$, or deep below the lead Fermi level, $\varepsilon_d < -U$, a negative differential conductance may appear in the vicinity of the first threshold bias voltage. Finally, figure 1(f) emphasizes the fact that TMR may change its sign along the ε_d-axis. Such a TMR inversion appears in linear as well as in nonlinear response regimes. Note also that TMR is enhanced in the vicinity of the threshold bias voltages. This enhancement occurs for positive as well as for negative TMR ratio at $\varepsilon_d > -U/2$ and at $\varepsilon_d < -U/2$, respectively. The width of the TMR peaks is determined by the magnitude of the spin-flip rate R, i.e. it depends on the distance between the corresponding split conductance peaks in figure 1(e).

Proceed now to analyze selected cross-sections of the maps in figure 1 in relation to the I–V characteristics calculated for other values of the spin-flip rate R. Our further calculation will also include spin precession on the dot, the magnitude of which may be evaluated from the non-vanishing off-diagonal occupation numbers given by equation (29). In addition, the influence of the lead spin polarization on the spin-valve effect in the presence of coherent rotations of electron spin on the dot, and the R-dependent modification of the rectification effect in asymmetrical junctions will also be briefly discussed.

4.2. Linear response regime, $V \approx 0$

Consider a symmetric tunneling junction in the equilibrium situation. In figure 2 the behavior of the linear conductance and the corresponding TMR is shown for selected values of the parameter R. As stated earlier, when $R = 0$, the linear conductance has peaks at resonance energies $\varepsilon_d = 0$ and $\varepsilon_d = -U$. It is also clearly seen that the conductance is symmetric at $\varepsilon_d = -U/2$. Due to higher-order tunneling transitions taking place in the equilibrium situation, the corresponding TMR ratio is enhanced in the whole range of the ε_d parameter except for the resonance energies. If weak spin-flip processes

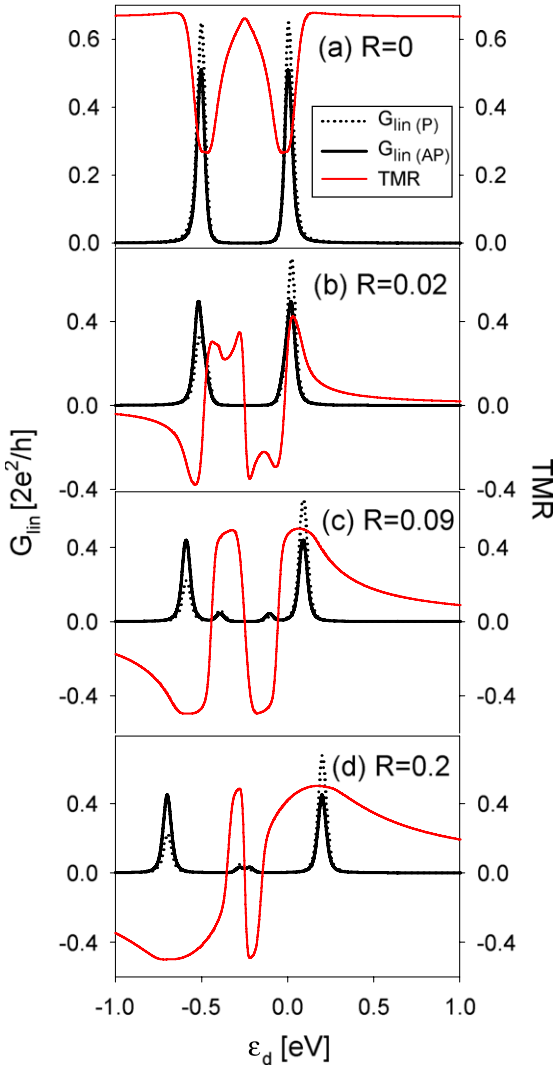

Figure 2. Linear conductance in the parallel, $G_{\mathrm{lin(P)}}$ (black solid line), and antiparallel, $G_{\mathrm{lin(AP)}}$ (black dotted line), configuration and TMR (red solid line) as a function of the QD energy level for selected spin-flip rates R (eV). The cross-sections of the maps in figure 1, taken at $V = 0$ correspond to the case $R = 0$ (a) and $R = 0.2$ eV (d). The other parameters are as in figure 1.

are involved, $R \approx \Gamma_\nu$, the symmetry of the conductance is broken in the P configuration and the height of the resonance peaks is diminished; however, still only a single conductance peak appears (see figure 2(b)). When the incident electrons tunnel coherently from the source lead onto the discrete level split by the coherent intradot spin rotation then, as displayed in figures 2(c) and (d), with increasing R two separate peaks become visible at resonances. To clearly establish the effects due to tunneling through the spin channels $\varepsilon_d \pm R$ and $\varepsilon_d + U \pm R$ we have taken $U > 2R$ for calculations. One should also point out the asymmetry of the split resonance peaks in figures 2(c) and (d). The latter results from the fact that an electron may tunnel from the source lead into two different states on the dot. These two states are determined, according to the equation (8), by the tunneling terms $T^\nu_{k\uparrow} a^\dagger_{\nu k\uparrow}(d_\uparrow + d_\downarrow)$ and $T^\nu_{k\downarrow} a^\dagger_{\nu k\downarrow}(d_\downarrow - d_\uparrow)$. The difference in height of the split conductance peaks visible in figures 2(c) and (d) follows from

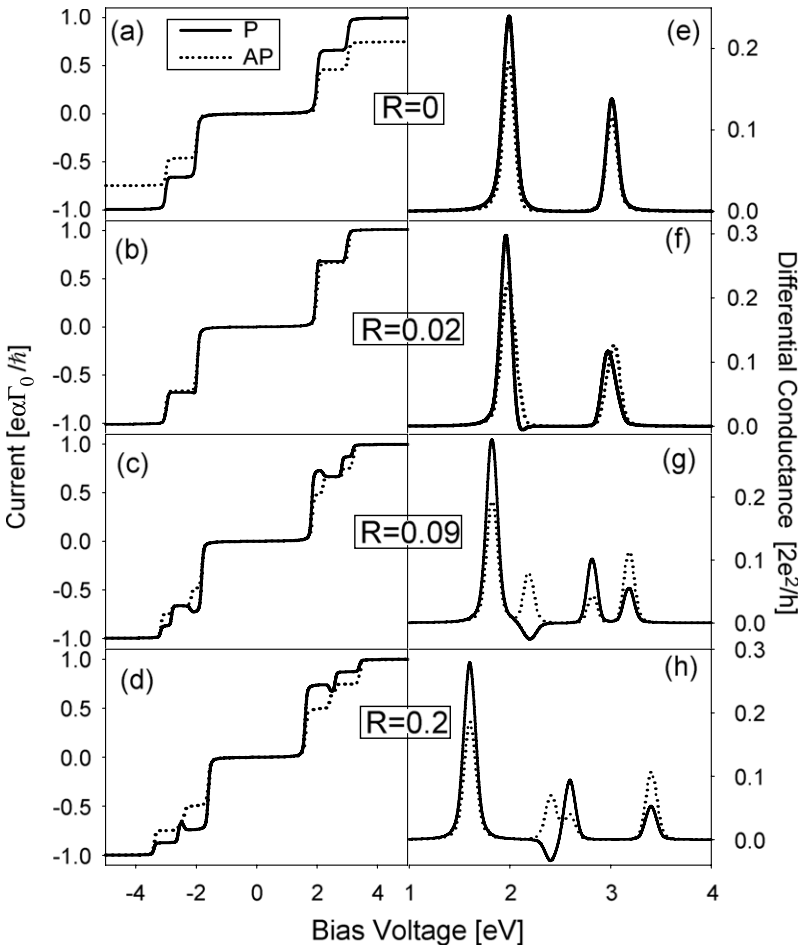

Figure 3. Bias dependence of the electric current ((a)–(d)) and differential conductance ((e)–(h)) for the symmetric junction in the parallel (solid lines) and antiparallel (dotted lines) configuration, for selected spin-flip rates R (eV). For clarity the differential conductance is displayed only for positive bias voltages. The dot energy is $\varepsilon_d = 1$ eV and the other parameters are as in figure 1.

the fact that one of the mentioned dot states (more precisely the one to which down-spin electrons are tunneling) is weakly coupled to the leads.

The competition between the level splitting, Coulomb correlations on the dot and the broadening of the split levels that arises from the tunneling coupling to the leads dominates the resonant behavior of the linear conductance of the system, and the latter in turn determines the TMR features. In particular, it is seen that TMR inversion at each resonance occurs and the amplitude of the TMR ratio changes from -50% up to 50%. Effectively, such an enhancement is larger than in the case of $R = 0$, where the TMR increases 30% above its minima at $\varepsilon_d = 0$ and $-U$. It is worth noting that TMR inversion in the presence of coherent spin-flip transitions on the dot has been predicted previously in magnetic tunnel junctions in the Kondo temperature regime [7, 8]. The change in sign of TMR at a gate voltage where the differential conductance peak is observed has also been detected experimentally beyond the Kondo regime in a hybrid device based on semiconductor InAs QD coupled to Ni electrodes. It is reported that the TMR value is changed from positive (30%) to negative (-60%). The sign changed TMR effect was basically interpreted in terms of the spin-dependent resonant tunneling model [61]. It was shown that the transmission probabilities calculated for strongly asymmetric coupling of the QD to the leads (which was the case for the experimental setup) gave rise to the negative TMR. Taking the present discussion into account, one may also suggest tunneling into superposition of the up-spin and down-spin states on the dot as another possible mechanism responsible for the observed TMR inversion.

4.3. Nonlinear response regime, $V \neq 0$

In discussion of the nonequilibrium situation we start with the symmetric junction, assuming in the following that the dot energy level is always empty in the corresponding equilibrium situation, i.e. $\varepsilon_d > 0$ at $V = 0$.

The electric current and differential conductance in the absence of intradot spin-flip processes, $R = 0$, taken for $\varepsilon_d = 1$ in equilibrium is displayed in figures 3(a) and (e), respectively. As described in the preceding section 4.1, the first and second steps in the current appear as a result of single and double occupancy of the dot, respectively. The corresponding differential conductance experiences two resonance peaks, which are clearly visible in figure 3(e), where for better clarity only the maxima for positive bias polarization are displayed. In

turn, figure 3(b) shows that for weak spin-flip transition rates, $R \approx \Gamma_\nu$, the electric current in the AP configuration tends to the current in the P configuration and the quantities J^{P} and J^{AP} are practically indistinguishable. The differential conductance in figure 3(f) reveals, however, that besides the distinct peak at first threshold bias voltage a small dip also appears at the $2(\varepsilon_{\mathrm{d}} + R)$ bias voltage, indicating that the QD discrete level is spin-split. On the other hand, at second threshold still only single peak in the corresponding differential conductance in figure 3(f) is visible.

The current behavior changes diametrically when stronger intradot spin-flip processes are involved. It is seen in figures 3(c) and (d) that with increasing R additional steps in the current in the vicinity of both the thresholds appear. The latter property is even better illustrated by the well-defined split peaks of the differential conductance in figures 3(g) and (h). It is seen also that in the P configuration the behavior of the current around the first threshold bias voltage differs from that observed at the second threshold. The first step in the current takes the form of a bump of width $2R$, which gives rise to two differential conductance peaks, one of which appears as a maximum at bias voltage $2(\varepsilon_{\mathrm{d}} - R)$, while the second one at $2(\varepsilon_{\mathrm{d}} + R)$ appears as a dip of negative value. The origin of such a behavior may be explained as follows. For the singly occupied dot, the sequential current becomes enhanced around the first threshold if electrons start to tunnel sequentially into a superposition of up- and down-spin states on the dot, namely into the dot state related to the tunneling term $T^{\nu}_{k\uparrow} a^{\dagger}_{\nu k\uparrow}(d_\uparrow + d_\downarrow)$ in equation (8). This scenario holds until with increasing bias electrons are also allowed to tunnel into the dot state determined by the term $T^{\nu}_{k\downarrow} a^{\dagger}_{\nu k\downarrow}(d_\downarrow - d_\uparrow)$. As discussed earlier, the latter dot state is weakly coupled to the leads so that a suppression of the electronic transmission arises, forming the bump in the current–voltage characteristics. This is in contrast to the situation at the second threshold, where an interplay between the spin-flip processes and Coulomb correlations on the dot results in the flat additional step in the current. Its plateau extends between the bias voltages $2(\varepsilon_{\mathrm{d}} + U \pm R)$ at which the differential conductance experiences the two maxima clearly visible in figures 3(g) and (h). In the AP configuration the difference in spin asymmetry for tunneling rates across the left and right barriers results in a lesser current enhancement and the additional steps in the current give rise to double conductance maxima at both thresholds.

The discussed differences between the currents in the P and AP geometries lead to TMR peaks of width $2R$ around the threshold bias voltages. Figure 4 shows that beyond these maxima, in particular above the second threshold, TMR is almost entirely reduced (see the cases of $R > 0$ in figure 4). Between the thresholds TMR suppression is also significant. The R-dependency of the latter phenomenon is illustrated in more detail in the inset of figure 4, where TMR as a function of R is displayed for the transport bias voltage fixed at 2.5 eV. Notice that after a significant TMR suppression a slight enhancement of TMR for larger spin-flip rates arises, which is simply due to the R-dependent widening of the TMR maximum around the second threshold. Hence, one may expect that with increasing Coulomb correlations on the dot, TMR suppression between the thresholds would be even more pronounced. Figure 4 shows also suppression of the central TMR peak below the first threshold bias voltage. It is seen that in the assumed limit of $R \gtrsim \Gamma_\nu$ the TMR suppression is diminished with increasing R. This implies that intradot spin rotation contributes to charge fluctuations on the dot thus inducing coherent electron transmission through virtual dot energy levels.

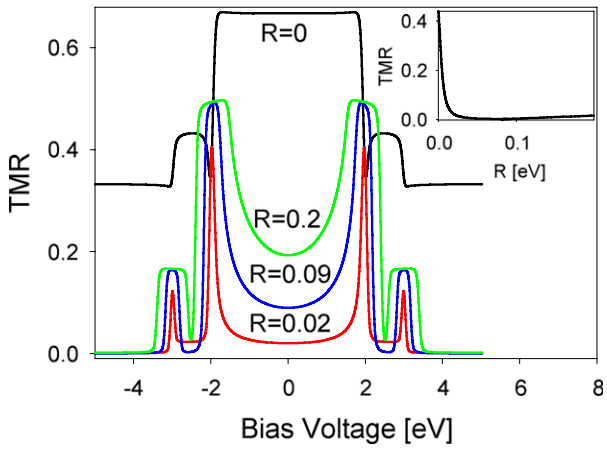

Figure 4. Bias dependence of TMR for indicated spin-flip rates R (eV). The other parameters are as in figure 3. The inset shows the R-dependence of TMR for the bias voltage fixed at 2.5 eV.

It is known that when spin rotation processes are involved the transverse spin components which are related to the off-diagonal occupation numbers via equation (32) may be accumulated on the dot, leading to spin precession around the direction perpendicular to the easy axis of the electrodes. As follows from figure 5, the magnitude of the off-diagonal occupation numbers strongly depends on the magnitude of the spin-flip rate. By using equations (16)–(29) it is predicted that with increasing R the magnitude of $n_{\sigma-\sigma}$ becomes three or even four orders smaller than the values calculated for diagonal occupation numbers n_σ. One may expect then that in the regime of $R \geqslant \Gamma_\nu$ assumed here, accumulation of the transverse spin components on the dot would have a rather minor influence on the electric current transmission.

4.4. Mesoscopic devices with half-metallic electrodes

4.4.1. Spin valve. Assume now that instead of ferromagnetic external leads, the quantum dot is coupled to half-metallic (fully polarized in one direction) electrodes, $p_{\mathrm{l}} = p_{\mathrm{r}} = 1$. If $R = 0$, then in contrast to the situation shown in figure 3(a) such a tunneling junction works as a perfect spin-valve device. More specifically, by rotating the lead magnetizations one may control the flow of electric current from the maximum value for the fully 'open' spin valve in the P configuration up to the entirely blocked current in the AP case [43, 46]. By definition (38), for the collinear alignment of magnetic moments of the leads the TMR ratio becomes then infinite.

Figure 6(a) compares electric currents calculated for the system with $R = 0$ (see the inset) with the current curves obtained for the same junction but with the spin-flip rate fixed

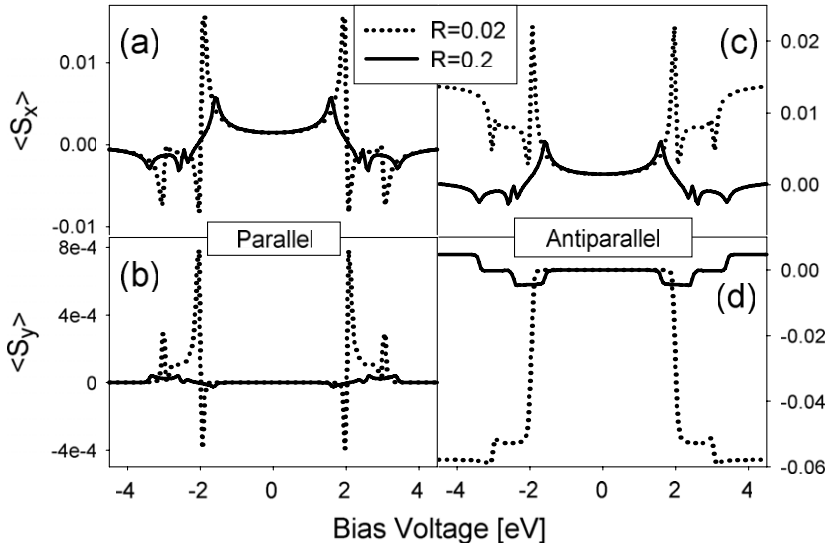

Figure 5. Bias dependence of the averages of the spin transverse components for the symmetrical junction in the parallel and antiparallel configuration, and for two selected values of the spin-flip rate R: $R = 0.02$ eV (dotted line) and $R = 0.2$ eV (solid line). The other parameters are as in figure 3.

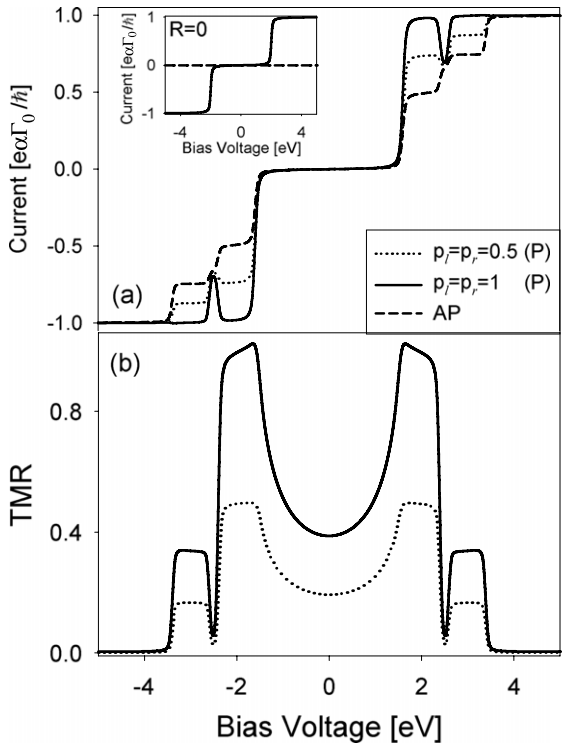

Figure 6. Bias dependence of electric current (a) and TMR (b) for the symmetric junction with the intradot spin-flip rate fixed at $R = 0.2$ eV. Electric current in the P configuration and TMR, calculated for the junction with the lead polarizations $p_l = p_r = 0.5$ (dotted lines) are compared to those obtained for the system with half-metallic electrodes, $p_l = p_r = 1$ (solid lines). The I–V characteristics in the AP configuration (dashed lines) overlap for the both lead polarizations. The inset shows electric currents for the spin-valve device with half-metallic electrodes, in the absence of spin-flip transitions, $R = 0$. The parameters ε_d, U, Γ_0 and T are as in figure 3.

at $R = 0.2$ eV. First, notice that if in the AP configuration electrons tunnel from the source into the superposition of up-spin and down-spin states on the dot, then further tunneling processes to the fully spin-polarized drain lead in the opposite direction become possible. Thus, spin-flip transitions lift the current blockade in the AP configuration and also make the quantity J^{AP} independent of the magnetic polarization of the leads. This is in contrast to the situation observed in the P configuration. When one compares the J^P curves for $p_l = p_r = 0.5$ (dotted line) and $p_l = p_r = 1$ (solid line) then it is clearly seen that the bump around the first threshold is enhanced for the system with half-metallic external leads. Thus, the TMR ratio takes a finite maximum value, approximately 100% larger than the TMR maximum observed in figure 4 for the junction with ferromagnetic leads.

4.4.2. Mesoscopic diode. Finally, consider a spintronic device offering the electric current rectification effect. This may be realized for a dot coupled via non-equivalent barriers to two different external leads, at least one being ferromagnetic. Here for calculations we take $\alpha = 0.1$ and $p_l = 0.4$, $p_r = 1$, i.e. it is assumed that the right electrode is made of a half-metallic material with electrons being totally spin-polarized at the Fermi level, whereas the factor $\alpha = 0.1$ indicates that on average electrons can tunnel much more easily to (from) the left electrode than to (from) the right one. The basic transport property of such an asymmetric tunneling junction is the asymmetry of its current–voltage characteristics with respect to the bias reversal. To be more precise, the tunneling junction under discussion may work as a mesoscopic diode. Prototypes of such a device were proposed in a number of theories [6, 38, 49, 59] and very recently realized experimentally for a system based on a carbon nanotube coupled to one ferromagnetic and one nonmagnetic external electrode [53]. Here, the typical diode-like behavior in the tunneling junction with arbitrary Coulomb correlations on the dot and with vanishing spin-flip transitions is represented by figures 7(a) and (e). For positive bias (the right lead is the source electrode), the current flows for both parallel

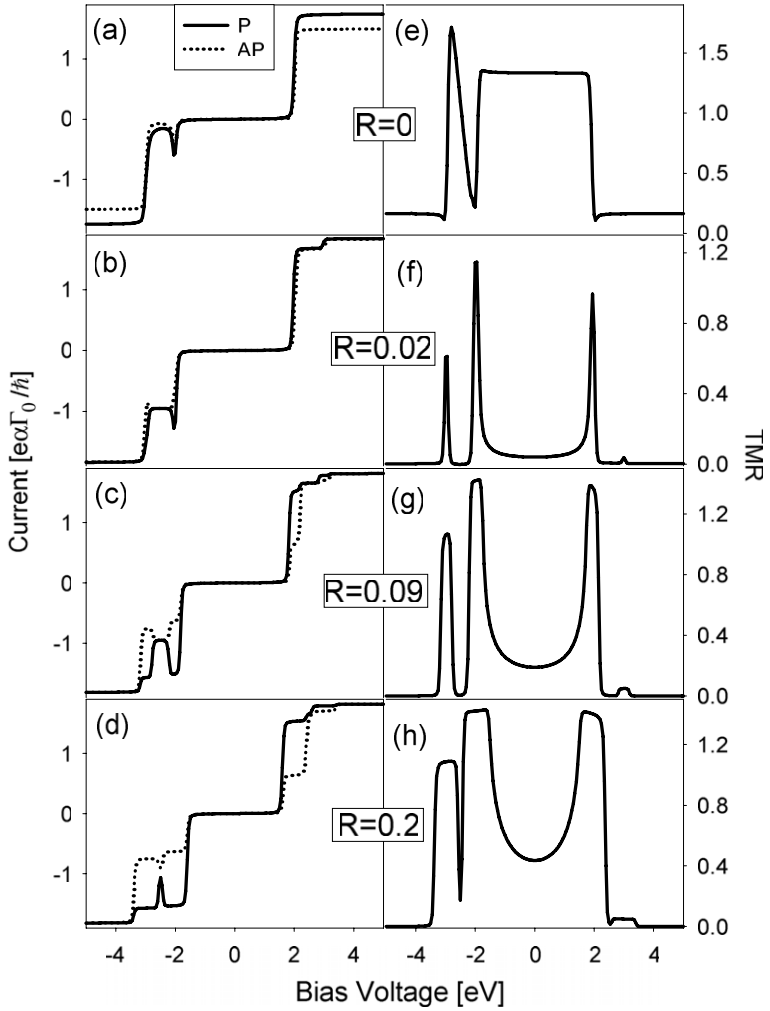

Figure 7. Bias dependence of electric current ((a)–(d)) and magnetoresistance ((e)–(h)), calculated for asymmetrical tunneling junction in the P and AP configuration and for indicated values of the parameter R (eV). The parameters assumed for numerical calculations are $\varepsilon_d = 1$ eV, $U = 0.5$ eV, $\Gamma_0 = 0.01$ eV, $p_l = 0.4$, $p_r = 1$, $\alpha = 0.1$ and $T = 100$ K.

and antiparallel configurations and thus TMR is significantly suppressed. By contrast, when electrons tunnel through the dot from the left electrode to the right (half-metallic) one, then below the first threshold voltage sequential tunneling is exponentially suppressed. At a sufficiently large bias voltage the energy level ε_d enters the tunneling window, and electric current starts to flow through the junction. This takes place only in a small voltage range in the vicinity of the first threshold voltage, where the resonant bump is observed. Above the bump, the current is suppressed by an electron residing on the dot and thus a significant enhancement of TMR is observed between the two threshold bias voltages. Finally, when $\varepsilon_d + U$ crosses the Fermi level of the source lead, the current increases again to saturate at a certain level.

Figures 7(b)–(d) show that even weak spin-flip transitions give rise to a suppression of the diode effect. Such a process proceeds differently for the currents in the P and AP configurations. At negative bias the variation of J^{AP} between the two thresholds is non-monotonic with increasing R, while the R-dependent variation of the J^{P} current in the same bias voltage range is monotonic. Moreover, the suppression of the TMR between the thresholds, appearing with increasing R, is accompanied by the enhancement of TMR around the second threshold. An analogous TMR behavior is visible at positive bias; however, in this case a larger transmission for majority and minority electrons makes the effect of the TMR enhancement much less pronounced. Interestingly, the TMR ratio predicted in the vicinity of the first threshold shows that coherent spin-flip processes may induce TMR maxima exceeding the results observed at $R = 0$. For the parameters used here it is found that the additional steps in the currents at the first threshold give rise to TMR maxima approximately 10% larger than the TMR plateau in figure 7(e).

5. Summary and conclusions

Spin-polarized transport through a single-level interacting quantum dot weakly coupled to ferromagnetic leads has been studied by means of the nonequilibrium Green function approach applied in the Hartree–Fock approximation. We have analyzed the electric current, conductance and tunnel magnetoresistance as well as accumulation of the spin

components on the dot in the presence of spin-flip processes causing coherent rotations of electron spin on the dot.

A number of new features of the spin-valve device under discussion have been revealed in the nonlinear response regime. It was shown that when spin-flip transitions overwhelm tunneling processes then the electric current exhibits a complex step-like behavior in the vicinity of the threshold bias voltages. The latter property gives rise to such effects as negative differential conductance and splitting of the differential conductance peaks, as well as to enhancement of the corresponding TMR at bias voltage range between each pair of the split conductance maxima. The maps of the TMR ratio plotted in the $(eV-\varepsilon_d)$-plane also showed that due to intradot spin-flip transitions TMR is significantly suppressed in the areas where sequential electron tunneling takes place as well as in the Coulomb blockade regions where higher-order tunneling processes occur. Moreover, self-consistent calculation of the dot occupation numbers resulted in non-zero averages of the transverse spin components of an electron residing on the dot. The latter indicates that spin-flip processes on the dot may be accompanied by spin precession around the direction perpendicular to the easy axis of the external electrodes.

Effects such as a spin valve for a QD coupled to identical half-metallic electrodes and the diode-like behavior observed for a QD coupled via non-equivalent barriers to one ferromagnetic and one half-metallic electrode have been proved to be suppressed in the presence of intradot spin flips. In the former case the non-zero current in antiparallel configuration gives rise to finite TMR opposed to an infinite TMR ratio in a system without spin-flip processes. In turn, in the case of the mesoscopic diode, spin flips lead to a reduction of the asymmetry in the current with respect to the bias reversal. Our calculations also reveal that reduction of the diode effect is accompanied by appearance of TMR maxima that may even exceed the TMR ratios observed for the system without intradot spin-flip transitions.

Finally, TMR inversion is found in the linear as well as nonlinear response regimes. In particular, TMR oscillation is predicted to occur in the linear limit and it is shown that TMR is inverted within each resonance of the linear conductance. Similar qualitative behavior has been reported in previous theories describing spin-polarized transport in the Kondo and co-tunneling regimes and has also been observed in recent experiments on spin-polarized electronic transport through InAs QDs coupled to Ni electrodes [52].

Acknowledgment

This work was supported by funds of the Polish Ministry of Science and Higher Education as a research project in the years 2006–2009.

References

[1] Fujisawa T, Austing D G, Tokura Y, Hirayama Y and Tarucha S 2002 *Nature* **419** 278
[2] Sahoo S, Kontos T, Furer J, Hoffmann C, Gräber M, Cottet A and Schönenberger C 2005 *Nature* **1** 99
[3] Lambert N, Mahboob I, Pioro-Ladrière M, Tokura Y, Tarucha S and Yamaguchi H 2008 *Phys. Rev. Lett.* **100** 136802
[4] Gupta J A, Awschalom D D, Peng X and Alivisatos A P 1999 *Phys. Rev.* B **59** R10421
[5] Khaetskii A V and Nazarov Y V 2000 *Phys. Rev.* B **61** 12639
[6] Rudziński W and Barnaś J 2001 *Phys. Rev.* B **69** 085318
[7] Zhang P, Xue Q-K, Wang Y and Xie X C 2002 *Phys. Rev. Lett.* **89** 286803
[8] López R and Sánchez D 2003 *Phys. Rev. Lett.* **90** 116602
[9] Hayashi T, Fujisawa T, Cheong H D, Jeong Y H and Hirayama Y 2003 *Phys. Rev. Lett.* **91** 226804
[10] Elzerman J M, Hanson R, Willems van Beveren L H, Witkamp B, Vandersypen L M K and Kouwenhoven L P 2004 *Nature* **430** 431
[11] Ma J and Lei X L 2004 *Europhys. Lett.* **67** 432
[12] Cao X, Shi Y, Song X, Zhou S and Chen H 2004 *Phys. Rev.* B **70** 235341
[13] Gywat O, Engel H-A, Loss D, Epstein R J, Mendoza F M and Awschalom D D 2004 *Phys. Rev.* B **69** 205303
[14] Tackeuchi A, Ohtsubo R, Yamaguchi K, Murayama M, Kitamura T, Kuroda T and Takagahara T 2004 *J. Appl. Phys.* **84** 3576
[15] Johnson A C, Petta J R, Taylor J M, Yacoby A, Lukin M D, Marcus C M, Hanson M P and Gossard A C 2005 *Nature* **435** 925
[16] Petta J R, Johnson A C, Taylor J M, Laird E, Yacoby A, Lukin M D and Marcus C M 2005 *Science* **309** 2180
[17] Braun P-F, Marie X, Lombez L, Urbaszek B, Amand T, Renucci P, Kalevich V K, Kavokin K V, Krebs O, Voisin P and Masumoto Y 2005 *Phys. Rev. Lett.* **94** 116601
[18] Gurudev Dutt M V, Cheng J, Li B, Xu X, Li X, Berman P R, Steel D G, Bracker A S, Gammon D, Economou S E, Liu R-B and Sham L J 2005 *Phys. Rev. Lett.* **94** 227403
[19] Hanson R, Willems van Beveren L H, Vink I T, Elzerman J M, Naber W J M, Koppens F H L, Kouwenhoven L P and Vandersypen L M K 2005 *Phys. Rev. Lett.* **94** 196802
[20] Zhang L Y, Wang C Y, Wei Y G, Liu X Y and Davidović D 2005 *Phys. Rev.* B **72** 155445
[21] Laird E A, Petta J R, Johnson A C, Marcus C M, Yacoby A, Hanson M P and Gossard A C 2006 *Phys. Rev. Lett.* **97** 056801
[22] Weymann I and Barnaś J 2006 *Phys. Rev.* B **73** 205309
[23] Climente J I, Bertoni A, Goldoni G, Rontani M and Molinari E 2007 *Phys. Rev.* B **76** 085305
[24] Meunier T, Vink I T, Willems van Beveren L H, Tielrooij K-J, Hanson R, Koppens F H L, Tranitz H P, Wegscheider W, Kouwenhoven L P and Vandersypen L M K 2007 *Phys. Rev. Lett.* **98** 126601
[25] Heiss D, Schaeck S, Huebl H, Bichler M, Abstreiter G, Finley J J, Bulaev D V and Loss D 2007 *Phys. Rev.* B **76** 241306(R)
[26] Taylor J M, Petta J R, Johnson A C, Yacoby A, Marcus C M and Lukin M D 2007 *Phys. Rev.* B **76** 035315
[27] Koppens F H L, Nowack K C and Vandersypen L M K 2008 *Phys. Rev. Lett.* **100** 236802
[28] Souza F M, Jauho A P and Egues J C 2008 *Phys. Rev.* B **78** 155303
[29] Moodera J S, Kinder L R, Wong T M and Meservey R 1995 *Phys. Rev. Lett.* **74** 3273
[30] Parkin S S P, Roche K P, Samant M G, Rice P M, Beyers R B, Scheuerlein R E, O'Sullivan E J, Brown S L, Gucchigano J, Abraham D W, Lu Y, Rooks M, Trouilloud P L, Wanner R A and Gallagher W J 1999 *J. Appl. Phys.* **88** 5828
[31] Zhang X, Li B S, Sun G and Pu F C 1997 *Phys. Rev.* B **56** 5484
Wilczyński M and Barnaś J 2000 *J. Magn. Magn. Mater.* **221** 373

[32] Imamura H, Chiba J, Mitani S, Takanashi K, Takahashi S, Maekawa S and Fujimori H 2000 *Phys. Rev.* B **61** 46
[33] Yakushiji K, Mitani S, Takanashi K, Takahashi S, Maekawa S, Imamura H and Fujimori H 2001 *Appl. Phys. Lett.* **78** 515
[34] Majumdar K and Hershfield S 1998 *Phys. Rev.* B **57** 11521
[35] Barnaś J and Fert A 1998 *Phys. Rev. Lett.* **80** 2058
Barnaś J and Fert A 1998 *Europhys. Lett.* **44** 85
[36] Takahashi S and Maekawa S 1998 *Phys. Rev. Lett.* **80** 1758
[37] Brataas A, Nazarov Yu V, Inoue J and Bauer G E W 1999 *Eur. Phys. J.* B **9** 421
Wang X H and Brataas A 1999 *Phys. Rev. Lett.* **83** 5138
[38] Bułka B R 2000 *Phys. Rev.* B **62** 3186
[39] Świrkowicz R, Barnaś J and Wilczyński M 2002 *J. Phys.: Condens. Matter* **14** 2011
[40] Fransson J, Eriksson O and Sandalov I 2002 *Phys. Rev. Lett.* **88** 226601
[41] Bułka B R and Lipiński S 2003 *Phys. Rev.* B **67** 024404
[42] Lopez R and Sanchez D 2003 *Phys. Rev. Lett.* **90** 116602
[43] Braun M, König J and Martinek J 2004 *Phys. Rev.* B **70** 195345
[44] Weymann I, König J, Martinek J, Barnaś J and Schön G 2005 *Phys. Rev.* B **72** 115334
[45] Weymann I, Barnaś J, König J, Martinek J and Schön G 2005 *Phys. Rev.* B **72** 113301
[46] Rudziński W, Barnaś J, Świrkowicz R and Wilczyński M 2005 *Phys. Rev.* B **71** 205307
[47] Weymann I and Barnaś J 2006 *Phys. Rev.* B **73** 205309
[48] Świrkowicz R, Wilczyński M, Wawrzyniak M and Barnaś J 2006 *Phys. Rev.* B **73** 193312
[49] Souza F M, Euges J C and Jauho A P 2007 *Phys. Rev.* B **75** 166303
[50] Barnaś J and Weymann I 2008 *J. Phys.: Condens. Matter* **20** 423202
[51] Hamaya K, Masubuchi S, Kawamura M, Machida T, Jung M, Shibata K, Hirakawa K and Taniyama T 2007 *Appl. Phys. Lett.* **90** 053108
[52] Hamaya K, Kitabatake M, Shibata K, Jung M, Kawamura M, Hirakawa K, Machida T, Taniyama T, Ishida S and Arakawa Y 2007 *Appl. Phys. Lett.* **91** 022107
[53] Merchant C A and Markowić N 2008 *Phys. Rev. Lett.* **100** 156601
[54] Meir Y and Wingreen N S 1994 *Phys. Rev.* B **50** R4947
[55] Romano C L, Ulloa S E and Tamborenea P I 2005 *Phys. Rev.* B **71** 035336
[56] Awschalom D D, Loss D and Samarth N 2002 *Semiconductor Spintronics and Quantum Computation* (Berlin: Springer)
[57] Büttiker M 1983 *Phys. Rev.* B **27** 6178
[58] Engel H-A and Loss D 2001 *Phys. Rev. Lett.* **86** 4648
[59] Weymann I and Barnaś J 2008 *Appl. Phys. Lett.* **92** 103127
[60] Haug H and Jauho A-P 1996 *Quantum Kinetics in Transport and Optics of Semiconductors* (Berlin: Springer)
[61] Cottet A, Kontos T, Sahoo S, Man H T, Choi M-S, Belzig W, Bruder C, Morpurgo A F and Schönenberger C 2006 *Semicond. Sci. Technol.* **21** 11